Dynamic modelling of subgrid scalar dissipation rate in premixed and partially premixed flames with differential filter

Ferrante, Gioele; Chen, Zhi X.; Langella, Ivan

Important note
To cite this publication, please use the final published version (if applicable).
Please check the document version above.

Research Paper

Dynamic modelling of subgrid scalar dissipation rate in premixed and partially premixed flames with differential filter

Gioele Ferrante [a],*, Zhi X. Chen [b,c], Ivan Langella [a]

[a] *Faculty of Aerospace Engineering, Delft University of Technology, Kluyverweg 1, Delft, 2629 HS, The Netherlands*
[b] *State Key Laboratory of Turbulence and Complex Systems, College of Engineering, Peking University, Beijing, 100871, China*
[c] *AI for Science Institute (AISI), Beijing, 100080, China*

A B S T R A C T

Large eddy simulation (LES) paradigms are used in the present work to predict premixed and partially premixed turbulent flames with flamelets based thermochemistry and presumed filtered density function approach for turbulence-chemistry interaction modelling. The combustion model requires a closure for the scalar dissipation rate of a progress variable, in which a modelling constant must be chosen. The present work focuses on the computation of the model constant through dynamic procedures based on the scale-similarity assumption, which requires the application of test-filters. In particular, two test-filtering approaches for LES, based respectively on an algebraic formulation and a newly proposed differential equation, are tested for flame configurations at different levels of turbulence, and using block-structured and unstructured meshes. The analysis shows that the differential filter, unlike the algebraic one, is handled well in situations of weak turbulence at comparable computational costs. At higher turbulence conditions the outcome looks less dependent on the test-filter and mesh topology used, although quantitative differences in the behaviour of the dynamically-computed model constant are still observable and discussed. Further analyses to understand the behaviour of the two filters are presented in the paper.

1. Introduction

Accurate and cost-effective modelling approaches are required to aid the design of new-generation gas turbines, able to meet the low-emissions targets set by the Paris agreement. Computational fluid dynamics is a powerful tool to predict the complex flow features within this design process. Among various techniques, LES represents a viable compromise between affordable computational cost and accurate prediction of the turbulent flow field. In a LES, only large scales are resolved, with models to mimic the effect of the small, subgrid scale (SGS) motions. Since combustion is a small-scale phenomenon [1], the turbulence-combustion interaction must be modelled in a LES. Among common closures for turbulent reacting flows in the context of LES there are the artificially thickened flame method [2], the conditional moment closure [3–6], transported [7–9] and presumed [10–12] filtered density function (FDF) approaches, and the flamelet approaches [13–16], of which each has its own advantages and limitations. A more extensive overview of different modelling approaches for LES of reacting flows can be found elsewhere [1,17,18]. The present work focuses on a flamelet-based combustion modelling approach combined with a presumed FDF approach. In this approach,

a database of one-dimensional laminar premixed freely-propagating flames (flamelets) is used to describe all possible thermochemical states of the mixture. This database is accessed using four controlling variables, namely a Favre-filtered progress variable, $\tilde{c}$, to track the reaction progress, a mixture fraction, $\tilde{\xi}$, to track the mixedness level, and their respective subgrid variances σ_c^2 and σ_ξ^2, whose Favre-filtered transport equations are directly solved in the LES (e.g. see [19,20]). In this framework, the progress variable SGS scalar dissipation rate (SDR), $\widetilde{\varepsilon}_c$, was shown to be a critical parameter for the correct estimation of σ_c^2. This term represents the unresolved part of the filtered SDR, $\widetilde{N}_c$, defined as:

$$\bar{\rho}\tilde{N}_c = \overline{\rho}\widetilde{D}_c(\nabla\tilde{c}\cdot\nabla\tilde{c}) + \bar{\rho}\tilde{\varepsilon}_c, \qquad (1)$$

where ρ is the mixture density and $\widetilde{D}_c$ is the filtered diffusion coefficient of $\widetilde{c}$. Overbar and tilde symbols refer respectively to simple and Favre filtered operations. Models for $\widetilde{\varepsilon}_c$ are commonly proportional to the SGS variance and can be written in general form as:

$$\tilde{\varepsilon}_c = f_1\sigma_c^2/\beta_c, \qquad (2)$$

where β_c is a modelling constant and f_1 is a function that depends on turbulence and combustion parameters. Past works have shown that

---

* Corresponding author.
  E-mail addresses: g.ferrante@tudelft.nl (G. Ferrante), chenzhi@pku.edu.cn (Z.X. Chen), i.langella@tudelft.nl (I. Langella).

this function needs to account for the dissipation of both SGS turbulent and reactive processes and therefore simple approaches such as the linear-relaxation model are not suitable for this quantity [21]. In the present study the model originally proposed in [22] and then adapted for LES in [19–21] is used, and the reader is referred to these works for further details. The model constant β_c depends on flame curvature, diffusion and reaction processes, and is generally scale-dependent. Its choice is of crucial importance to obtain the correct estimation of SGS variance. Note that these considerations are generalizable also for other combustion model constants in different approaches, although they may signify different processes. Thus, while the use of a static value of the combustion constant may lead to good results, it requires an accurate preliminary tuning. Furthermore, the value might need to change in space and time for cases where the aforementioned processes or the numerical mesh (thus the LES filter) is not homogeneously distributed, and for such cases a single constant value might not be suitable. Relatively recently, scale similarity assumptions for modelling parameters such as flame wrinkling and flame surface density have been proposed and investigated, e.g. see [23–26]. Dynamic models based on the scalar dissipation rate have been also investigated [19,27]. Although these models were observed to work on different regimes, the assumption of scale similarity is arguable for reacting quantities, and it is unclear whether the application of dynamic modelling leads to correct estimation of the modelling constant. An example was provided in [28], where it was discussed that on unstructured meshes the classical test-filter approaches based on Gaussian shapes lead to excessive noise and incorrect results due to the pseudo-Fourier condition [29]. Nevertheless, to the best of the authors' knowledge, a thorough investigation of the influence of the test filter in dynamic modelling for combustion LES still does not exist. In the present work we aim to fill this knowledge gap by investigating different techniques for test filtering, and testing the outcomes on two different configurations at different levels of turbulence, in order to evaluate the performance for different turbulent kinetic energy spectra. In particular, classical test-filtering approaches are compared to the so-called differential filters, where the general test filtered quantity $\hat{\phi}$ is obtained through the resolution of a differential equation rather than the direct application of a Gaussian filter. This class of filters has been commonly used for non-reacting flows (e.g. see [30]), but not for reacting cases. In this work we discuss advantages and limitations of these as compared to algebraic approaches from both modelling and computational cost perspectives, for the case of a flamelets-based combustion closure where the model constant within the scalar dissipation rate of a progress variable is unknown. The analysis suggests that algebraic formulations give acceptable predictions at relatively high turbulence levels, while differential formulation provides good estimations for a much wider range of conditions and mesh types at the cost of a relatively marginal increase of computational effort.

The remainder of this paper is organized as follows. In Section 2 the combustion modelling and the dynamic procedures for the estimation of the model constant are presented and discussed. In Section 3 the two selected test cases are introduced, and further details of LES, meshes and boundary conditions are reported. Results for the two cases are discussed in Section 4. A further discussion on the numerical approaches for dynamic modelling is presented in Section 5. Concluding remarks are provided in Section 6.

2. Modelling

2.1. LES and combustion modelling

The Favre-filtered, density varying Navier–Stokes equations for reacting flows are, in Einstein's notation:

$$\frac{\partial \overline{\rho}}{\partial t} + \frac{\partial \overline{\rho}\widetilde{u}_j}{\partial x_j} = 0 \tag{3}$$

$$\frac{\partial \overline{\rho}\widetilde{u}_i}{\partial t} + \frac{\partial \overline{\rho}\widetilde{u}_i\widetilde{u}_j}{\partial x_j} = -\frac{\partial \overline{p}}{\partial x_i} + \frac{\partial}{\partial x_j}\left(\widetilde{\mu}\frac{\partial \widetilde{u}_j}{\partial x_j}\right) - \frac{\partial \widetilde{\tau}_{ij}}{\partial x_j} \tag{4}$$

$$\frac{\partial \overline{\rho}\widetilde{h}}{\partial t} + \frac{\partial \overline{\rho}\widetilde{u}_j\widetilde{h}}{\partial x_j} = \frac{\partial}{\partial x_j}\left(\overline{\rho}\widetilde{D}_T\frac{\partial \widetilde{h}}{\partial x_j}\right) - \frac{\partial \widetilde{\tau}_h}{\partial x_j} \tag{5}$$

In the above equations, u_i is the velocity component in direction i, p is the modified pressure, μ is the dynamic viscosity estimated via Sutherland's law, $\mathcal{D}_T$ is the thermal diffusivity, h is the specific absolute enthalpy (sum of formation and sensible enthalpies), x_i is the coordinate in direction i and t represents time. The Favre-filtered temperature $\widetilde{T}$ is computed from enthalpy by inverting the following relation:

$$\widetilde{h} = \widetilde{\Delta h}_f^0 + \int_{T_0}^{T} \widetilde{C}_{p,\text{mix}}(T')\, dT' \tag{6}$$

where $C_{p,\text{mix}}$ and Δh_f^0 are the specific heat at constant pressure and the formation enthalpy at $T_0 = 298.15$ K of the mixture, respectively. Using the theorem of the integral mean, temperature can be found from Eq. (6) as $\widetilde{T} = T_0 + (\widetilde{h} - \widetilde{\Delta h}_f^0)/C_p^{eff}$, where $C_p^{eff} = \int_{T_0}^{T} C_p(T')dT'/(T - T_0)$ is the mixture effective specific heat capacity at constant pressure. A low-Mach approximation is used, for which density is computed from the operative pressure p_r and from temperature using the equation of state for ideal gases, $p_r = \overline{\rho}R_0\widetilde{T}/\widetilde{W}$, where R_0 is the universal gas constant and $\widetilde{W}$ is the molar mass of the mixture. All the introduced thermodynamic quantities, i.e. mixture molecular weight W, enthalpy of formation Δh_f^0 and effective specific heat C_p^{eff} are computed from 1D laminar flamelets, preintegrated and tabulated consistently with the presumed filtered density function framework explained later in this section.

The unresolved stress tensor, $\widetilde{\tau}_{ij}$ is closed using eddy diffusivity as $\widetilde{\tau}_{ij} = -2\overline{\rho}\nu_{sgs}\left(\widetilde{S}_{ij} - \widetilde{S}_{kk}\delta_{ij}/3\right)$, where $\widetilde{S}_{ij}$ is the Favre-filtered stress tensor and δ_{ij} is the Kronecker delta. The subgrid scale (SGS) viscosity in this equation is closed using a one-equation model as $\nu_{sgs} = C_\nu k^{1/2}\Delta$, where Δ is the LES filter width (estimated as the cubic root of the local cell volume in the computation), $C_\nu \approx 0.1$ is a model constant, and k is the SGS kinetic energy computed using the following transport equation [31,32]:

$$\frac{\partial \overline{\rho}k}{\partial t} + \frac{\partial \overline{\rho}\widetilde{u}_j k}{\partial x_j} \approx \frac{\partial}{\partial x_j}\left(\widetilde{\mu}\frac{\partial k}{\partial x_j}\right) + \widetilde{u}_i\frac{\partial(\widetilde{\tau}_{ij} + 2k\delta_{ij}/3)}{\partial x_j} - \frac{\partial f_j}{\partial x_j} \tag{7}$$

In the above equation, $f_j = \overline{\rho}(\widetilde{u_j u_i u_i} - \widetilde{u}_j\widetilde{u_i u_i})/2 \approx C_f\overline{\rho}\Delta\sqrt{k}(\partial k/\partial x_j)$ is the turbulent transport of k and $\epsilon_k \approx C_\epsilon\overline{\rho}k^{3/2}/\Delta$ its SGS dissipation rate. The values of the model constants are $C_\epsilon = 1.048$ and $C_f = 0.094$. The pressure-work term was shown to be negligible in the context of the SGS stress modelling [32] and therefore it is not considered in the equation for k. Finally, a gradient hypothesis is assumed for the unresolved transport of h, i.e. $\widetilde{\tau}_h = -(\nu_T/\text{Pr}_T)\partial\widetilde{h}/\partial x_j$.

In order to close the above set of equations, a combustion model is needed. A flamelet assumption is used in the present work, i.e. the flame is assumed to be thin enough that the smallest turbulent scales can only wrinkle and corrugate the flame, without affecting its internal structure. This way the turbulent flame can be seen as an ensemble of thin, one-dimensional laminar flames, whose thermochemical structure can be computed a priori. It was shown in many past works (e.g [33, 34]) that in the context of LES the flamelet assumption holds for a wide range of combustion regimes, including relatively high Karlovitz numbers. This is because at high Karlovitz numbers the turbulent flame can still be seen as an ensemble of locally thin laminar flames distributed in space, leading to a broad flame brush. In the present work the thermochemical state is assumed to be dependent only on the reaction progress and the mixedness level. The latter is estimated using the Bilger's mixture fraction [35], whose Favre-filtered transport equation reads:

$$\frac{\partial \overline{\rho}\widetilde{\xi}}{\partial t} + \frac{\partial \overline{\rho}\widetilde{u}_j\widetilde{\xi}}{\partial x_j} = \frac{\partial}{\partial x_j}\left(\overline{\rho}\widetilde{D}_\xi\frac{\partial \widetilde{\xi}}{\partial x_j}\right) - \frac{\partial \widetilde{\tau}_\xi}{\partial x_j} \tag{8}$$

with $\widetilde{\tau}_\xi$ representing the SGS transport of ξ, which is closed using a gradient hypothesis as for the enthalpy equation. It is worth noting

that the diffusivity of ξ, D_ξ, is assumed to be that of species under the assumption of unity Lewis number. Despite one of the case investigated involves hydrogen, additional analyses (not shown) using models for differential diffusion [36,37] have shown that differential diffusion effects can be neglected for this relatively high turbulence case given the objectives of the present work, therefore the unity Lewis number assumption is retained here for simplicity.

The reaction progress is estimated using a scaled progress variable, defined as $c = \sum Y_k(\xi)/\max(\sum Y_k(\xi))$, where $\sum Y_k$ is a suitable combination of species k with mass fraction Y_k and $\max(\sum Y_k(\xi))$ refers to the equilibrium value. Following previous works [20,34,38,39], the sum of CO_2 and CO is used here when the fuel is a hydrocarbon, and the mass fraction of water vapour is used when the fuel is hydrogen. This choice guarantees a monotonic behaviour of the progress variable as the reaction progresses, at least for the cases under investigation, which is essential for the correct behaviour of the flamelet modelling. In either cases and in the assumption of unity Lewis number, the Favre-filtered transport equation for c is:

$$\frac{\partial \overline{\rho}\widetilde{c}}{\partial t} + \frac{\partial \overline{\rho}\widetilde{u}_j\widetilde{c}}{\partial x_j} = \frac{\partial}{\partial x_j}\left(\overline{\rho}\widetilde{D}_c\frac{\partial \widetilde{c}}{\partial x_j}\right) - \frac{\partial \widetilde{\tau}_c}{\partial x_j} + \overline{\dot{\omega}}_c \tag{9}$$

where D_c is the diffusivity of c, taken equal to D_ξ under the unity Lewis number assumption, and $\widetilde{\tau}_c$ is again closed using a gradient hypothesis. The last term in the above equation is the filtered reaction rate of c. Since the flame in the cases to be investigated in the present work is not resolved, $\overline{\dot{\omega}}_c$ cannot be directly taken from the laminar solution, as one has to take into account the SGS wrinkling effect by turbulence. A filtered density function (FDF) approach is used here to close this term [18,40]:

$$\overline{\dot{\omega}}_c(\widetilde{c},\widetilde{\xi},\sigma_c^2,\sigma_\xi^2) = \overline{\rho}\int_0^1\int_0^1\frac{\dot{\omega}_c}{\rho}P(c,\xi;\widetilde{c},\widetilde{\xi},\sigma_c^2,\sigma_\xi^2)\,dc\,d\xi + \overline{\dot{\omega}}_{np} \tag{10}$$

where $\dot{\omega}_c$ is the reaction rate in Arrhenius form taken from the laminar one-dimensional solution and $P(c,\xi)$ is the joint FDF of c and ξ, whose shape depends on the Favre-filtered values of c and ξ and their respective SGS variances, σ_c^2 and σ_ξ^2. Following previous works [41–43], the joint FDF is presumed as the product of two β functions, i.e. $P(c,\xi;\widetilde{c},\widetilde{\xi},\sigma_c^2,\sigma_\xi^2) \approx P_c(c;\widetilde{c},\sigma_c^2)P_\xi(\xi;\widetilde{\xi},\sigma_\xi^2)$. The above assumption implies statistical independence at the SGS level of c and ξ, which was shown to be satisfactory in the context of LES [18,40,41]. The term $\overline{\dot{\omega}}_{np}$, appearing in Eq. (10), is a correction factor to account for the non-premixed mode contribution in inhomogeneous flows, and is computed as [44]:

$$\overline{\dot{\omega}}_{np} \approx \overline{\rho}\widetilde{c}(\widetilde{D}_\xi\nabla\widetilde{\xi}\cdot\nabla\widetilde{\xi} + \widetilde{\varepsilon}_\xi)\int_0^1\int_0^1\frac{1}{\psi^b(\xi)}\frac{d^2\psi^b(\xi)}{d\xi^2}P(c,\xi)\,dc\,d\xi \tag{11}$$

where ψ^b is the value of progress variable on the burnt side for each value of ξ and $\widetilde{\varepsilon}_\xi$ is the SGS scalar dissipation rate (SDR) of ξ, which is modelled using linear relaxation as $\widetilde{\varepsilon}_\xi = c_\xi(v_t/\Delta^2)\sigma_\xi^2$, with $c_\xi \approx 2$ [26].

The SGS variances of c and ξ are estimated in this work using their respective transport equations:

$$\frac{\partial \overline{\rho}\sigma_\xi^2}{\partial t} + \frac{\partial \overline{\rho}\widetilde{u}_j\sigma_\xi^2}{\partial x_j} = \nabla\cdot\left[\overline{\rho}\left(\widetilde{D}_\xi + \frac{v_t}{Sc_t}\right)\nabla\sigma_\xi^2\right] - 2\overline{\rho}\widetilde{\varepsilon}_\xi + 2\overline{\rho}\frac{v_t}{Sc_t}\left(\nabla\widetilde{\xi}\cdot\nabla\widetilde{\xi}\right) \tag{12}$$

$$\frac{\partial \overline{\rho}\sigma_c^2}{\partial t} + \frac{\partial \overline{\rho}\widetilde{u}_j\sigma_c^2}{\partial x_j} = \nabla\cdot\left[\overline{\rho}\left(\widetilde{D}_c + \frac{v_t}{Sc_t}\right)\nabla\sigma_c^2\right] - 2\overline{\rho}\widetilde{\varepsilon}_c + 2\overline{\rho}\frac{v_t}{Sc_t}\left(\nabla\widetilde{c}\cdot\nabla\widetilde{c}\right) + (\overline{\dot{\omega}_c c} - \overline{\dot{\omega}}_c\widetilde{c}) \tag{13}$$

where the gradient hypothesis for the SGS transport terms is already appearing in the equations, $Sc_t \approx 0.7$ is the SGS Schmidt number, and the last term in Eq. (13) is modelled consistently to Eq. (10). The subgrid SDR of c in Eq. (13) is modelled with Eq. (2), where f_1 is computed as [22,42]:

$$f_1 = \left[1 - \exp\left(\frac{-0.75\Delta}{\delta_{th}}\right)\right]\left[(2K_c - \tau C_4)\frac{s_L}{\delta_{th}} + C_3'\frac{\epsilon_k}{k}\right] \tag{14}$$

In the above equation s_L, δ_{th} and τ are respectively laminar flame speed, thermal thickness and heat release factor, and are obtained from the flamelets. Other parameters are non-tuneable, the reader can find more information in [20,42].

2.2. Dynamic estimation of model constant

The value of the model constant β_c in Eq. (2) might vary in space depending on the local flow conditions. In such cases dynamic approaches can be used to avoid the fine-tuning of the modelling constant. Dynamic approaches have been employed in LES as an effective method to model subgrid quantities and are based on the scale similarity assumption [45]. These methods have been largely used for non reacting flows to model the subgrid stress tensor through the knowledge of the neighbouring smallest resolved scales (Germano's identity) [46]. The concept of similarity between the smallest resolved scale and the unresolved scales comes in this case from the argument of the turbulence cascade within the inertial range of the turbulent kinetic energy (TKE) spectrum, and is enforced in the LES by the use of a test filter width about twice that of the smallest resolved scale. In case of reacting flows the application of such procedures is less trivial due to the energy release by the flame at the small scales. Nevertheless, the applicability of scale-similarity was shown to still hold for a number of different modelling approaches including flame wrinkling, flame surface density, and scalar dissipation rate [19,25,32,47–50].

A dynamic procedure for the modelling of the subgrid scalar dissipation rate is employed here, following previous works e.g. [19]. By indicating the filtered scalar dissipation rate of c with $\widetilde{N}_c \equiv D_c\overline{\nabla c \cdot \nabla c} = \widetilde{D}_c\nabla\widetilde{c}\cdot\nabla\widetilde{c} + \widetilde{\varepsilon}_c$, the application of scale similarity to the next (test-filter) scale reads

$$\widehat{\overline{\rho}\widetilde{N}_c} - \widehat{\overline{\rho}}\widehat{\widetilde{D}}_c\nabla\widehat{\widetilde{c}}\cdot\nabla\widehat{\widetilde{c}} = \widehat{\overline{\rho}}f_1(\widehat{\mathbf{q}})\frac{\widehat{\sigma}_c^2}{\widehat{\beta}_c} \tag{15}$$

where $f_1(\mathbf{q})\sigma_c^2/\beta_c$ is the functional form used for $\widetilde{\varepsilon}_c$, the symbol $\widehat{}$ indicates the test-filter operation and $\mathbf{q} \equiv (k,\epsilon_k,\Delta,\ldots)$ is the entire set of spatially-varying parameters to which f_1 depends on. By using Germano's identity, the left-hand side of above equation can be rewritten as:

$$\left(\widehat{\overline{\rho}\widetilde{D}_c\nabla\widetilde{c}\cdot\nabla\widetilde{c}} + \widehat{\overline{\rho}f_1(\mathbf{q})\frac{\sigma_c^2}{\beta_c}} - \widehat{\overline{\rho}\widetilde{D}_c\nabla\widetilde{c}\cdot\nabla\widetilde{c}}\right) + \left(\widehat{\overline{\rho}\widetilde{D}_c\nabla\widetilde{c}\cdot\nabla\widetilde{c}} - \widehat{\overline{\rho}}\widehat{\widetilde{D}}_c\nabla\widehat{\widetilde{c}}\cdot\nabla\widehat{\widetilde{c}}\right)$$

$$= \widehat{\overline{\rho}f_1(\mathbf{q})\frac{\sigma_c^2}{\beta_c}}$$
$$+ \left(\widehat{\overline{\rho}\widetilde{D}_c\nabla\widetilde{c}\cdot\nabla\widetilde{c}} - \widehat{\overline{\rho}}\widehat{\widetilde{D}}_c\nabla\widehat{\widetilde{c}}\cdot\nabla\widehat{\widetilde{c}}\right)$$

At this point β_c can be found in two ways. In the first case, one assumes that it is scale-invariant, i.e. $\widehat{\beta}_c = \beta_c$, and the equation can be solved explicitly as

$$\beta_c = \frac{\widehat{b} - a}{L} = \frac{\widehat{\overline{\rho}f_1\sigma_c^2} - \widehat{\overline{\rho}}\widehat{f_1}\widehat{\sigma}_c^2}{\widehat{\overline{\rho}}\widehat{\widetilde{D}}\nabla\widehat{\widetilde{c}}\cdot\nabla\widehat{\widetilde{c}} - \widehat{\overline{\rho}\widetilde{D}\nabla\widetilde{c}\cdot\nabla\widetilde{c}}}, \tag{16}$$

where the parameters $b = \overline{\rho}f_1\sigma_c^2$, $a = \widehat{\overline{\rho}}\widehat{f_1}\widehat{\sigma}_c^2$ and $L = \widehat{\overline{\rho}}\widehat{\widetilde{D}}\nabla\widehat{\widetilde{c}}\cdot\nabla\widehat{\widetilde{c}} - \widehat{\overline{\rho}\widetilde{D}\nabla\widetilde{c}\cdot\nabla\widetilde{c}}$ have been introduced for simplicity. On the other hand, the assumption of scale-invariance might be too restrictive as β_c was found in previous studies to actually depend on the filter size, as discussed earlier. As an alternative, one can relax this assumption by rewriting Eq. (15) as:

$$\widehat{\beta}_c = -\frac{a}{L - \widehat{b/\beta_c}} = -\frac{\widehat{\overline{\rho}}\widehat{f_1}\widehat{\sigma}_c^2}{\left(\widehat{\overline{\rho}}\widehat{\widetilde{D}}\nabla\widehat{\widetilde{c}}\cdot\nabla\widehat{\widetilde{c}} - \widehat{\overline{\rho}\widetilde{D}\nabla\widetilde{c}\cdot\nabla\widetilde{c}}\right) - \widehat{\overline{\rho}f_1(\mathbf{q})\frac{\sigma_c^2}{\beta_c}}} \tag{17}$$

The above equation needs an estimation for β_c on the right-hand side of the equation, which is usually taken in LES solvers from the previous

time step or the previous iteration (if more than one per time step). On the other hand, a minimum number of iterations is required for the iterative process to converge, which limits the application of this method.

Another issue related to the applications of Eqs. (16) and (17) is that a test filter has to be chosen. In the context of non-reactive simulations with eddy-viscosity type closures it was shown that the LES filter is similar to a Gaussian filter when the LES is well resolved (minimal influence of mesh), and approaches a box filter as the mesh coarsens [45]. The choice of the test filter has of course impact on the calculation of the β_c parameter. In the present study an algebraic and a differential filter are compared. The test-filtering operation on the general, spatially-varying quantity ϕ is described by the following convolution operation

$$\hat{\phi}(x) = \int_{\mathcal{V}} \phi(x') \mathcal{F}(x - x') \, dx' \tag{18}$$

where $\mathcal{V}$ is the integration volume and $\mathcal{F}$ is the test filter function. In the algebraic case, the test filter is obtained by imposing a shape function (usually a Gaussian shape) of a certain width, taken to be twice the LES filter width in the present work. After discretization the above integral assumes the general form:

$$\hat{\phi} = \frac{\sum_k A_k^f \phi_k^f}{\sum_k A_k^f}, \tag{19}$$

where A_k^f are weight coefficients evaluated on the numerical cell and its surrounding cells. The issue with this formulation is that the evaluation of both coefficients A_k^f and function values ϕ_k^f is subject to interpolation errors, which may become particularly relevant on unstructured meshes [28].

Following [28,51] the convolution within the filtering operation can be expanded in series of Taylor around the value at point x. Without loss of generalities, for the one-dimensional case and assuming a symmetric filter, this would read as

$$\hat{\phi}(x,t) = \phi(x,t) + \frac{\hat{\Delta}^2}{24} \frac{\partial^2}{\partial x^2} \phi(x,t) + \mathcal{O}(\Delta^4) \tag{20}$$

Similarities with the Fourier diffusion differential equation can be noted. Solving this equation directly can however lead to numerical instabilities (Pseudo Fourier conditions). In the present work it is proposed to solve this equation implicitly in the finite volumes framework within the time marching integration. In order to do so, the quantity $\hat{\phi}(x,t)$ can be seen as the solution of the following differential equation:

$$\frac{d\hat{\phi}(\mathbf{x},t)}{dt} = \frac{\Delta_x^2}{6\Delta_t} \nabla^2 \hat{\phi}(\mathbf{x},t). \tag{21}$$

where Δ_t is the LES time step, and $\hat{\Delta} = 2\Delta_x$ has been used, with $\Delta_x = \mathcal{V}^{1/3}$ being the LES filter width estimated as the cubic root of the local cell volume $\mathcal{V}$. Eqs. (20) and (21) are equivalent to the third order if the latter is solved with an implicit Euler time marching scheme. The advantage of solving the differential equation is that it can be embedded within the finite volume framework therefore minimizing the noise produced by interpolation errors, at the cost of additional computational effort.

3. Test cases and numerical details

For the analysis in the present work, two test cases are selected. The first, Case A (Fig. 1, left), is the lifted jet flame in hot vitiated coflow developed by Cabra et al. [52]. This setup consists of a central nozzle issuing a fuel mixture composed of 25% H_2 and 75% N_2 in volume. The bulk velocity of the fuel stream is 107 m/s, allowing for a significant amount of turbulence to develop in the shear region downstream the nozzle exit. The hot coflow in this configuration is issued at 1045 K and is composed of the products of lean H_2/air flame at an equivalence ratio

of $\phi = 0.25$ (H_2O, O_2 and N_2). This case is characterized by relatively high Reynolds number and a relatively wide turbulent kinetic energy spectrum.

The second case, Case B (Fig. 1, right), is the lean premixed, bluff-body stabilized flame studied in [53]. In this set-up, a low bulk velocity stream of 5 m/s of methane/air mixture at equivalence ratio $\phi = 0.75$ and inlet temperature $T_{in} = 300$ K is issued into a cylindrical duct with confinement ratio $R_{out}/R_{in} = 2$. The Reynolds number based on the bluff body diameter $D = 25$ mm is Re = 7950. This configuration leads to moderate levels of turbulence in the bluff body wake, where a recirculation zone is formed, which is *ad hoc* to compare the ability of the dynamic models for relatively narrow energy spectrum.

The two cases, summarized in Tables 1–2, are simulated using an *in-house* solver developed in OpenFOAM v9, which uses the finite volume approach and a low-Mach approximation to solve the reacting Navier–Stokes equations along with the four transport equation for the controlling variables discussed in Section 2. The Pressure-Implicit with Splitting Operator (PISO) loop [54] is used for the pressure-velocity coupling, with a minimum of 5 additional outer iterations per time step for the other equations. An implicit Euler scheme is used for time marching along with a time step ensuring that the CFL number is below 0.3 everywhere in the domain. Second order schemes are used for the spatial gradients, with Gamma limiters [55] in the region of the flame where strong gradients are present. The numerical domains for the two cases are sketched in Fig. 1.

Two block-structured meshes of 0.9 and 2.6 million hexahedral cells are generated using Ansys ICEM CFD software and used for cases A and B, respectively. Additionally, case A is also simulated on a tetrahedral computational grid of 3.3 million cells to investigate the effects of the test filter also when an unstructured mesh is in use. Each grid is refined within the flame region to have a ratio between filter size and laminar flame thickness of about 1. The Pope criterion is employed [56] to assess that at least 80% of the total turbulent kinetic energy falls within the resolved scales and ensure a suitable grid resolution. For this purpose midplane contours of the ratio $k_{sgs}/(K + k_{sgs})$ are shown in Fig. 2, where k_{sgs} is the subgrid kinetic energy taken from its transport equation and K is the resolved turbulent kinetic energy. The contour plots show that the modelled k_{sgs} falls below the 20% of the total turbulent kinetic energy in the regions of interest of the domain, i.e around the flame. It has to be noted that high values of this ratio are encountered at the walls, where most of the kinetic energy in the boundary layer is modelled through wall functions, and in low turbulence regions of the domain, where both k_{sgs} and K approach zero, which also explains the relatively larger values observed for case B (bluff body).

For case A, constant ambient pressure is imposed at the outlet and at the lateral cylindrical surface, while zero normal gradient condition is imposed to the other quantities. Constant temperature conditions are imposed at the jet and coflow inlet according to Table 1, and a constant axial velocity of 3.5 m/s is imposed at the coflow inlet. A synthetic eddies generator [57] is used to impose a time-varying turbulent velocity profile at the jet inlet. A target mean velocity profile and rms velocity profile are imposed according to the measurements reported in [58–60]. The flame lift-off height was observed to be very sensitive to the turbulent inlet condition [58] and a value for the integral turbulent length scale l_0 must be accurately chosen. As no experimental characterization is available for this quantity, a sensitivity analysis was performed and a value of $l_0 = 0.07D$ was selected for the block-structured mesh, as it was observed to provide a good representation of jet spreading, and good agreement with measured averaged and rms mixture fraction and velocity profiles. A mesh sensitivity analysis (reported in the Appendix Section) and the Pope's criterion for turbulent kinetic energy reported in Fig. 2 show that the block-structured and the unstructured meshes have similar level of refinement and are able to resolve most of the turbulent kinetic energy. However, the instantaneous velocity conditions produced by the synthetic eddies

Table 1
Operating conditions of the lifted hydrogen flame case.

	D [mm]	U_{bulk} [m/s]	Re	T [K]	X_{H_2}	X_{O_2}	X_{N_2}	X_{H_2O}
Jet	4.57	107	23-600	305	0.25	–	0.7427	–
Coflow	210	3.5	18-600	1045	–	0.1474	0.7534	0.0989
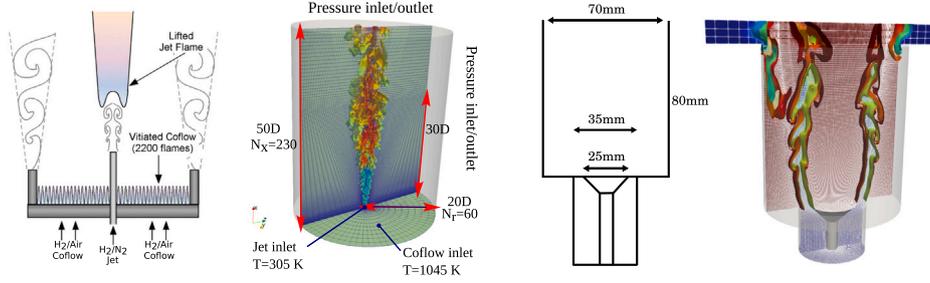
Fig. 1. Sketches and rendering from LES of the piloted jet lifted flame of Cabra et al. [52] (left) and the premixed, low-turbulence bluff-body flame of Dawson et al. [53] (right).
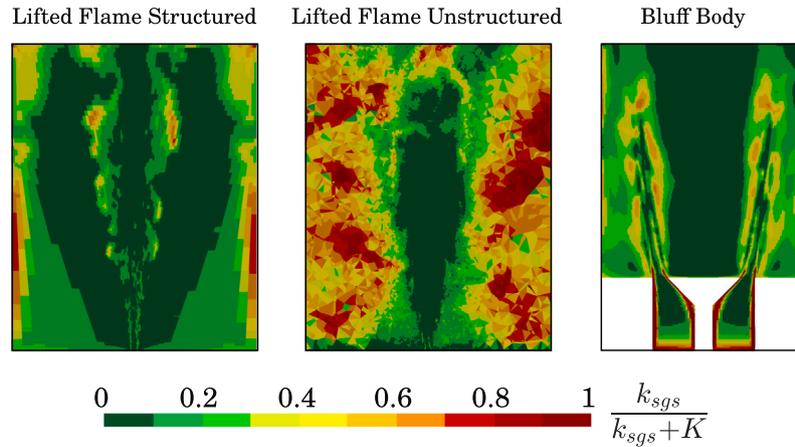
Fig. 2. Pope criterion: ratio of the subgrid kinetic energy k_{sgs} (from turbulence model) and total turbulence kinetic energy (K resolved + modelled).

Table 2
Operating conditions of the bluff body case.

	U_{bulk} [m/s]	Re	T [K]	ϕ	X_{CH_4}	X_{O_2}	X_{N_2}
Reactants	5 m/s	7950	300	0.75	0.073	0.194	0.733

generator can be dependent on the selected mesh, also for same values of the integral length scale. For this reason, to obtain similar turbulent velocity field (mean and rms velocity) near the nozzle exit $x = 1D$, where experimental measurements are available, a value of $l_0 = 0.05D$ was imposed for the unstructured mesh. On the two meshes, the comparisons between the two test filter strategies, which represent the objective of the present work, are conducted at the same integral length scale value.

For case B, a plenum is located downstream of the flame region to prevent influence of the outlet boundary conditions on the flame and constant ambient pressure is imposed at its outlet. Adiabatic boundary conditions are used for temperature and enthalpy at the wall and no-slip conditions for the velocity. Spalding wall functions are used for the turbulent viscosity at the wall [61].

The precomputed and tabulated thermochemistry is built on pre-mixed freely propagating laminar 1D flamelets at given reactants conditions. The calculation is performed using the CHEM1D solver [62] together with GRI3.0 mechanism [63] for the methane-air flame (case B) and San Diego mechanism [64] for the hydrogen flame (case A). A unity Lewis number is considered for every species when modelling the diffusive transport in both test cases. Under this assumption, the

mixture fraction value is constant along a single flamelet and equal to its value in the reactants.

Respectively 100 and 50 points are used in the precomputed table for the progress variable space (varying between 0 and 1) and its SGS variance (varying between 0 and $c(1 - c)$). For case B a single methane-air flamelet at an equivalence ratio of $\phi = 0.75$ and reactants temperature of $T_{reac} = 300$ K is considered. For Case A (lifted jet flame in hot coflow), also mixture fraction and its SGS variance are among the control variables, therefore a database of 300 freely propagating premixed flamelets is built, with reactants equivalence ratios spanning the flammability range, corresponding to a mixture fraction range $\xi = [0.1, 0.75]$ and stoichiometric conditions at $\xi_{st} = 0.474$. In this case, the mixture fraction represents the mixing between jet and coflow streams. Therefore, the reactants temperature and species mass fractions vary linearly with the mixture fraction, between their value in the coflow (oxydiser stream $\xi = 0$), to their value in the jet (fuel stream $\xi = 1$), as reported in Table 1.

When tabulated, the mixture fraction ξ range is discretized with 160 linearly spaced points within the flammability limits, and its subgrid variance σ_ξ^2 is discretized using 15 exponentially-spaced points between 0 and $\xi(1 - \xi)$. Thermodynamic states outside the flammability limits are linearly interpolated between the values at the lean (rich) flammability limit and air (fuel) conditions.

A typical computation of a characteristic flow through time for cases A and B takes about 4k and 12.5k CPU-hours (on block-structured meshes), respectively, using 256 cores in parallel on a 2.6 GHz Intel Xeon processor architecture. The CPU time for the different strategies
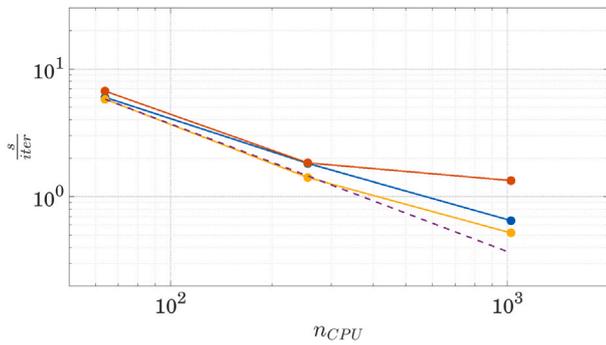
Fig. 3. Time required, in seconds per iteration, to compute the modelling parameter β_c using differential (—) and algebraic (—) test filters, for different number of CPU-cores, n_{CPU} used in parallel. The scaling obtained using a static (fixed) value of β_c (—) and the ideal scaling (– –) are also reported for reference.

for the definition of the model parameter are compared in Fig. 3. The two dynamic strategies show a similar computational cost, which is up to 26% higher than for the static case at 256 cores used in parallel. For larger number of cores the computation time using the differential filter is up to two times higher than for the algebraic filter due to non-optimized scalability within the algorithm currently implemented.

4. Results

The objective in this section is to understand capabilities of the differential test-filter of Eq. (21) in predicting the correct flow field as compared to the algebraic approach of Eq. (19). In order to have a detailed comparison and drive quantitative insights on the accuracy of the proposed filter, case A (lifted flame in hot coflow) is investigated first. In fact, a wide amount of data is available for this case from the experimental campaigns [52,65], which includes radial profiles of velocity, temperature and mixture fraction, allowing to validate the models proposed. This case is thus analysed next before the bluff-body case. Note that the modelling constant β_c in Eq. (2) is evaluated for both test-filter approaches by the use of Eq. (16). Further considerations involving the use of Eq. (17) are given instead in Section 5.

4.1. Jet flame in hot coflow

This case is firstly analysed using the block-structured mesh in order to minimize possible interpolation errors in the computation of the coefficients in Eq. (19). An overview of the flow field as predicted by using the two test filters is presented in Fig. 4, showing midplane contours of temperature, modelling constant β_c, and SGS variance of c, σ_c^2. As can be seen from the figure, the β_c field as predicted by the differential test filter appears to be very similar to that predicted by the explicit algebraic formulation. This similarity is attributed to the aforementioned minimization of interpolation errors by the use of a block-structured mesh, and to the relatively high level of turbulence associated with the high bulk velocity of the fuel jet, leading to a relatively wide spectrum of scalar dissipation rate. Consequently, the instantaneous features of the subgrid variance of progress variable, whose value depends on the SDR, are also similar. The temperature contour in the same figure further reveals that the lift-off height is predicted similarly when either the algebraic or the differential filter are used. Radial profiles of mean mixture fraction, temperature, velocity, and their variances, shown in Fig. 5, further indicate that both filter methods perform very well as compared to the experimental data. The results above lead to the two important following observations:

1. An algebraic test filter holds well for reacting cases with a relatively high level of turbulence and block-structured meshes, even if the code used interprets any mesh as unstructured;

2. The model proposed in Eq. (21) mimics well the same flow field, indicating that this equation is consistent and accurate despite the truncation to the third order.

Now that the two test-filter approaches have been validated against experimental results, further investigations can be conducted by replacing the block-structured mesh with an unstructured one in order to assess whether there is any difference in the results obtained by the use of the two test filters. It is worth to note that the unstructured mesh is constructed to maintain the LES filter size in the region of the flame equal or very similar to that of the block-structured mesh, which is in turn of the order of the laminar flame thickness. This way the two test filters can be directly compared for the same filter width. Instantaneous flow features in terms of progress variable reaction rate, β_c and σ_c^2 are shown in Fig. 4 (top row). When the differential filter is used, the lift-off height on the unstructured mesh is predicted at about the same position estimated when the block-structured mesh was used (about 50 mm from the nozzle exit). Vice versa, when the algebraic filter is used, the lift-off height is predicted about 15 mm upstream. This is a consequence of somewhat lower values of β_c predicted in the latter case, resulting in lower values of SGS variance σ_c^2 (see Fig. 4, top-right), which in turn imply higher values of reaction rate in the flamelet model used and thus an acceleration of the flame towards more upstream positions. This shift is of course reflected in the statistics presented in Fig. 5. It is worth noting that overall better results are obtained by using the block-structured mesh as compared to the experimental data. Nevertheless, this result is biased by selection of the inlet turbulence length scale value imposed to the synthetic eddies generator. A fine tuning of this parameter for the unstructured mesh, however, goes beyond the scope of this work, where the objective is to mimic the main effect of the modelling constant on the SDR (and consequently the SGS variance), which for this configuration is immediately reflected on the flame liftoff height discussed above. It is also worth noting that unstructured meshes are known to introduce more numerical diffusion (for the same filter size) than block-structured meshes [26,66], which implies that the turbulence imposed at the nozzle exit may develop less quickly than for the block-structured mesh. The reader can find a mesh sensitivity analysis (for both BS and US meshes) and additional comments on this point in the Appendix Section.

Further insights on the behaviour of the model constant when algebraic and differential test filters are used is provided by looking at the distribution of β_c within the domain in Fig. 6. Values are collected using several time snapshot only for the regions within the flammability limits and with the further condition $0.05 \leq \tilde{c} \leq 0.95$ in order to exclude points outside the flame front. Note that, being β_c scale-dependent in principle, its distribution is expected to be different when different meshes are used, which is evident from the figure. Some differences between algebraic and differential test-filter methods in the distribution of the modelling parameter β_c are visible already for the block-structured mesh case. In particular, a clear peak is not clearly distinguishable in the logarithmic plot in the case of the algebraic filter. Nevertheless, the mean value of β_c predicted in the two cases is similar. By looking at the scatter plots and conditional mean of SGS scalar dissipation rate in Fig. 7 (right), one can notice indeed that this quantity is predicted equivalently for any value of SGS variance. Similar scatters are also observed, which explain why the statistics predicted on the block-structured mesh are very similar when the two test filters are used, despite the differences observed in Fig. 6. A different relative behaviour is observed instead for the unstructured mesh cases. Here the distribution of β_c in Fig. 6 (left) leads to an overall lower mean value in the case of the algebraic filter, consistently with the instantaneous field contours observed for Fig. 4. By looking at the conditional means of subgrid SDR in Fig. 7 (left), one can notice that now this quantity is overestimated when the algebraic test-filter is used. This larger SDR justifies the lower SGS variances observed in the contours of Fig. 4, and thus the acceleration of the flame upstream.
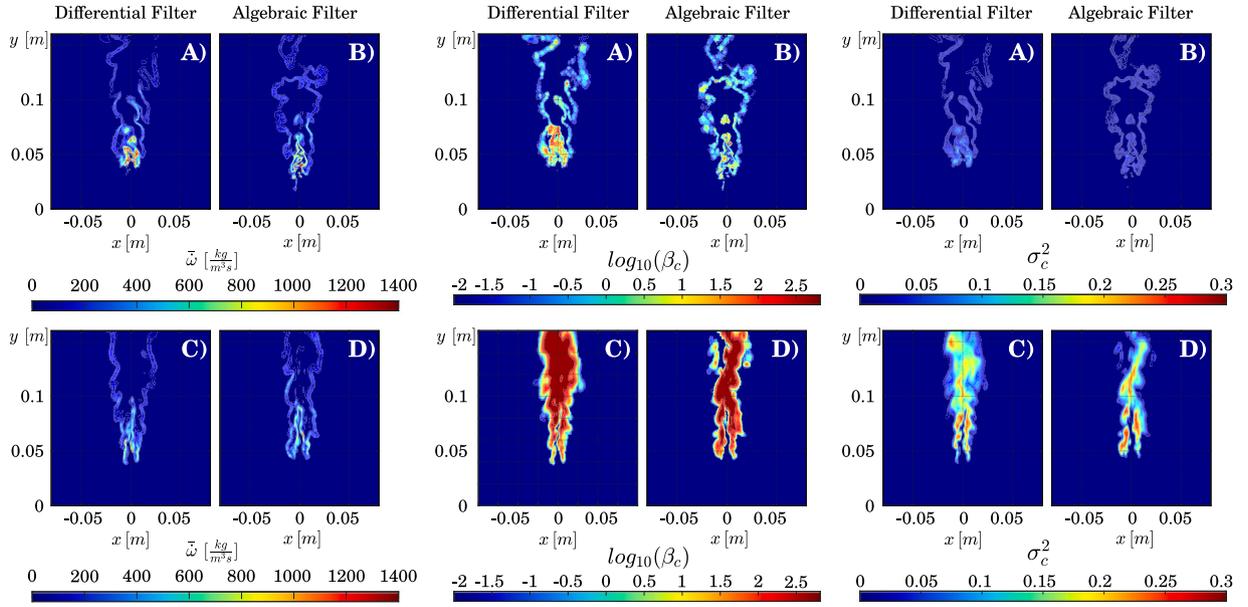
Fig. 4. Comparison between instantaneous fields of filtered reaction rate of progress variable (left), β_c parameter (centre) and SGS variance of progress variable σ_c^2 (right), as predicted using the algebraic and differential filters, for Case A (jet in hot coflow). Results are shown for the unstructured (top) and block-structured (bottom) meshes.
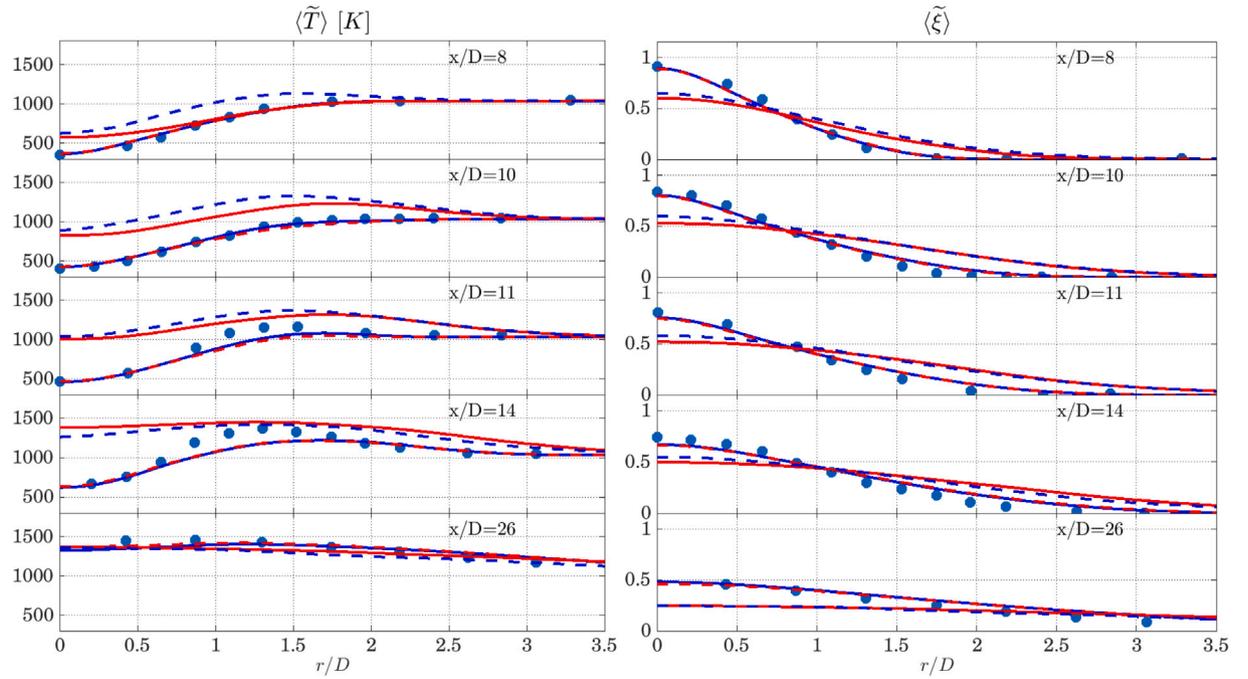

Fig. 5. Radial profiles of time averaged temperature and mixture fraction at different axial locations from experimental measurements (symbols) and LES: unstructured mesh with differential (—) and algebraic (- -) test filters; block-structured mesh with differential (—) and algebraic (- -) test filters.
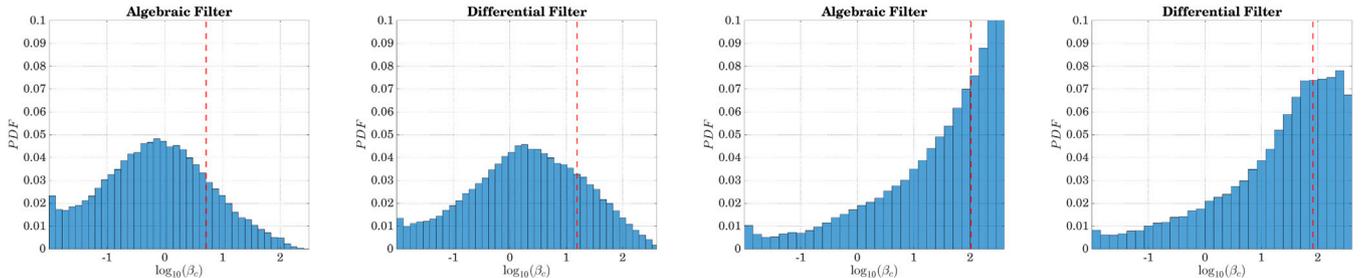
Fig. 6. Distribution of β_c in the lifted flame for the jet in hot coflow configuration (case A) for unstructured (left) and block-structured (right) meshes, obtained using differential and algebraic test filters. Vertical dashed lines indicate mean values.
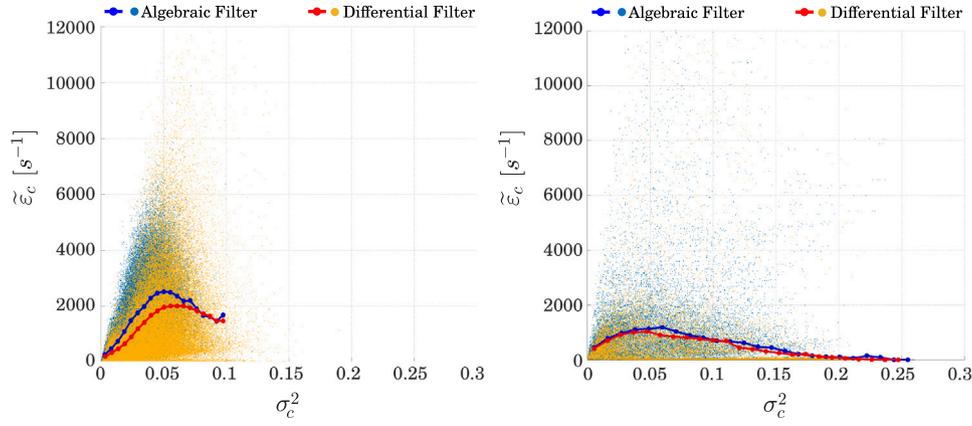
Fig. 7. Scatter plots of subgrid scalar dissipation rate of progress variable, $\widetilde{\varepsilon}_c$ versus subgrid variance of c, σ_c^2, as obtained on unstructured (left) and block-structured (right) meshes, for both algebraic and differential test filters. Conditional means are also shown.
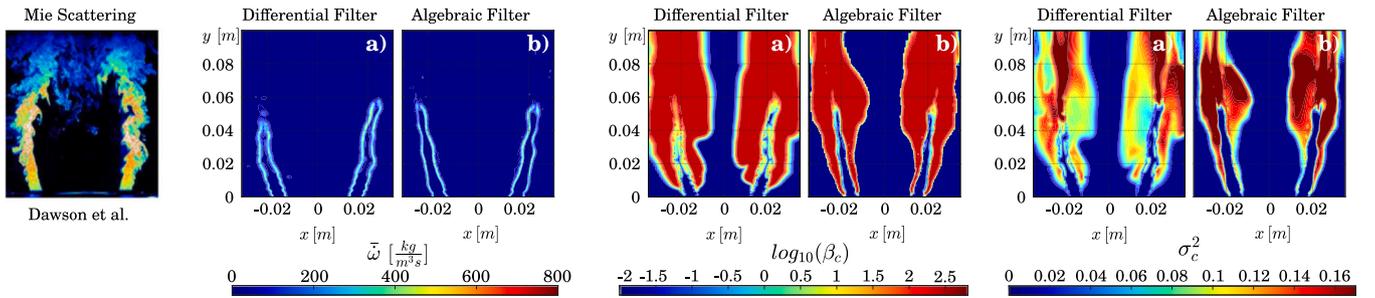

Fig. 8. Comparison between instantaneous fields of filtered reaction rate (left), β_c parameter (centre) and SGS variance of progress variable (right), as predicted using the algebraic and differential filters, for Case B (bluff-body stabilized flame) on block-structured mesh. Mie scattering images taken from [53] are also shown on the left for reference.

From the above analyses one can conclude that, for conditions of relatively high turbulence (implying relatively wide turbulent kinetic energy spectrum), the algebraic test filter provides similar results to the differential filter. Nevertheless, the differential filter outperforms the algebraic one in terms of accuracy, particularly on unstructured meshes (as observed for the lift-off prediction), which is attributed to the increased noise produced by interpolation operations for a fixed filter width, for such a mesh. For this reason, and by the investigation of the results presented, it is plausible to expect that as the mesh accuracy converges towards DNS size (cell volume $\mathcal{V} \rightarrow 0$) and interpolation errors become less relevant, the two test filters might converge to the same result. In the next Section it will be shown that different considerations apply in conditions of weak turbulence.

4.2. Weakly-turbulent bluff body stabilized flame

In [67] it was noted that a dynamic formulation for the estimation of β_c would not hold in conditions of weak turbulence due to the limited range of turbulence scales available. The weakly turbulent premixed case investigated experimentally in [53] (Case B in this work) is thus chosen to further assess the capabilities of algebraic and differential test filters in predicting the correct values of the combustion modelling constant within the subgrid SDR model of Eq. (2). Only the block-structured mesh as discussed in Section 3 is used. The use of an unstructured mesh is expected in fact to affect the outcomes in terms of accuracy as observed for the jet flame in case B. Since relative differences in the flow field are already observed when using the two test-filters on the block-structured mesh for this case as will be discussed next, the use of an unstructured mesh for similar LES filter size is expected to amplify these differences and therefore this analysis is not repeated here.

Midplane contours of filtered temperature, β_c distribution (in logarithmic scale) and subgrid variance σ_c^2 as predicted by using algebraic

and differential filter methods on the block-structured mesh are shown for the bluff-body case in Fig. 8. Unlike the jet flame in hot coflow case, here the two test-filter methods lead to different results also using the block-structured mesh. When the algebraic test filter is used, the dynamic procedure does not seem able to describe with sufficient resolution the local variations of the combustion model constant β_c across the flame region. This leads to significantly different distribution of subgrid variance, which in turns affects the resolved wrinkling of the flame as observed in the figure. By looking at the distribution of β_c in Fig. 9, one can notice that a well-defined peak value cannot be identified for the case of algebraic test-filter. Further inspection of the data shows that in many regions of the flame β_c oscillates between the imposed cutoff values, and $\beta_c \rightarrow 0$ in most of the domain (note that β_c in the numerical algorithm is truncated to $\varepsilon > 0$ to avoid a division by zero), implying a range of values across the flame is not predicted by the algebraic test-filter. This results in erroneous high values of the sub-grid SDR, and consequent low values of subgrid variance, which in turn implies the flame behaves in large extent as a laminar flame. This is not the case in the experiments for this configuration, as could be seen from the OH-LIF and Mie scattering images reported in [53] (See Fig. 8, left). Previous studies [68] highlighted the importance of the flame turbulence interaction, describing how the flame assumes a laminar-like behaviour close to the base of the bluff body and contributes to turbulence generation further downstream in the shear layer. From the comparison with the calculated non-reacting flow field, the flame appears to damp the weak turbulence generated in the shear layer around the bluff body, as a result of thermal expansion. On the other hand, the use of the differential filter results in a better calculation of β_c which now assumes a well-defined range of different local values across the flame front (Fig. 8), and a clear peak in its distribution is present (Fig. 9). Consequently, higher values of σ_c^2 are obtained in the flame region. Note that also in this case the presence of the flame dumps the turbulence at the base of the bluff body, when compared to the
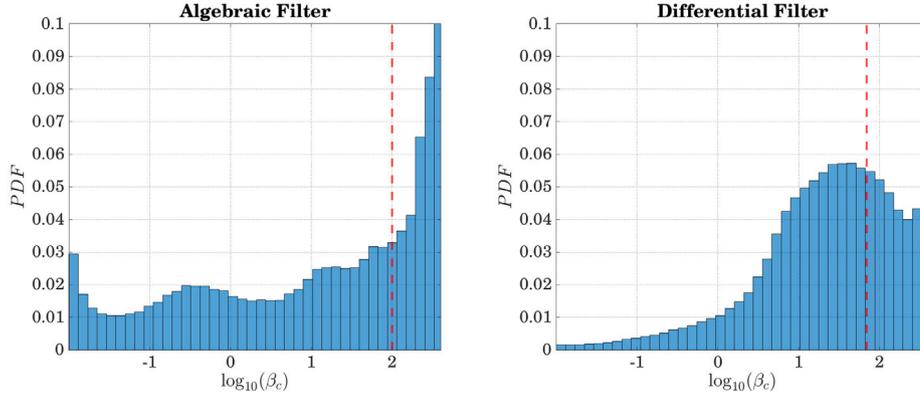
Fig. 9. Distribution of β_c over the flame front in the bluff-body stabilized flame (case B) obtained using differential and algebraic test filters applied on block-structured mesh. Vertical dashed line indicate the mean value.

non-reacting case (not shown). However, the formation of instabilities sustaining the turbulent structures in the shear layer can be observed further downstream in Fig. 8. By looking at the scatter plots of subgrid SDR in Fig. 10, it is found that the conditional SDR is overestimated in the case of the algebraic test-filter at low values of subgrid variance, while for values of σ_c^2 above about 0.04 algebraic and differential test-filters predict essentially the same result. This supports the argument that the two filters behaves differently in conditions of weak turbulence ($\sigma_c^2 \to 0$), and that the difference is caused by values of β_c saturating towards the lower cutoff limit at these conditions ($\beta_c \to 0$ implies larger values of $\widetilde{\varepsilon}_c$). This behaviour, from the numerical point of view of the test-filter algorithm, is similar to that observed in Fig. 7 for the unstructured mesh. However, in that case low values of β_c were produced by noise arising from interpolation accuracy, resulting in overestimation of $\widetilde{\varepsilon}_c$ for a wider range of values of σ_c^2. For the bluff body case investigated in this section, instead, overestimations of $\widetilde{\varepsilon}_c$ are observed only for relatively low values of σ_c^2, indicating that the issue is in the estimation of the model constant in quasi-laminar regions. It is worth noting that additional tests were conducted (not shown) using a static approach with a value of β_c imposed as the mean of the values obtained from dynamic procedure. These tests resulted in a quite different flame structure as compared to the results from dynamic approach, indicating that imposing a single value for the combustion parameter is not trivial for this turbulence-evolving study case, thus stressing out the relevance of using robust dynamic approaches for this kind of combustion configurations.

5. Numerical considerations on dynamic approaches

In Section 4 the estimation of the combustion modelling constant β_c was performed using Eq. (16) and the assumption of scale invariance. A question that might arise is whether this assumption has effect on the results presented, in particular the predictions obtained by the use of the algebraic test-filter. Additional considerations are therefore given in this section regarding the use of Eq. (17), where the assumption of scale invariance is relaxed. Additional simulations have been performed on this purpose on the bluff-body stabilized case (Case B) by using the algebraic test filter and replacing Eq. (16) with Eq. (17). It is worth noting that the value of β_c appearing on the left-hand side of Eq. (17) is not exactly the same of that appearing on the right-hand side, as the former appears under the test-filter operator symbol. In first instance, the two values are assumed to be the same. This way Eq. (16) and (17) are equivalent and only differ in the method used to solve for β_c. Further considerations about this assumption will be provided later in this section.

In order to solve Eq. (17), an iterative procedure needs to be applied. By defining $\alpha_c = 1/\beta_c$, this equation can be rewritten as:

$$\widehat{\alpha}_c \approx \alpha_c = \alpha_{c,n+1} = 1/\beta_{c,n+1} \approx \frac{\widehat{b}}{a}\alpha_{c,n} - \frac{L}{a} \tag{22}$$
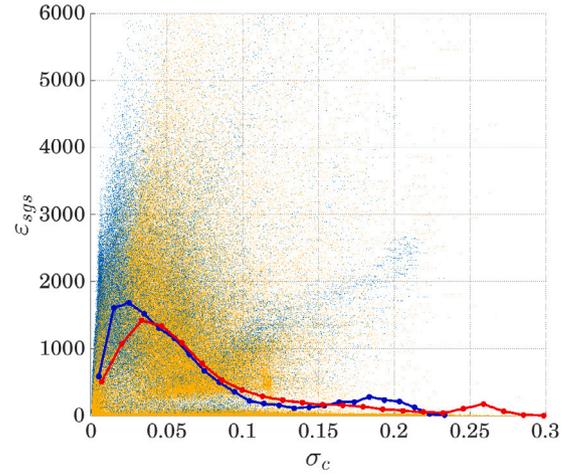

Fig. 10. Scatter plots of subgrid scalar dissipation rate of progress variable, $\widetilde{\varepsilon}_c$ versus subgrid variance of c, σ_c^2, as obtained on block-structured mesh for differential (●) and algebraic test filters (●). Conditional means are also shown: algebraic test filter (——), differential filter (——).

where due to scale invariance, α_c was taken outside the test-filter operation on the right-hand side of the equation, and n refers to the generic iteration number. This equation as written has the form of a fixed-point iterative equation with preconditioning, and always converges for values of $b/a < 1$. On the other hand, convergence needs more than one iteration. Assuming the initial guess is of the order of magnitude at least of the exact value (which could be the case by taking the modelling constant value from the previous time step in a LES), typically order of ten iterations are needed for α_c to converge to the exact value. This poses challenges in the implementation of Eq. (17) in numerical codes due to the increased computational cost. One can alternatively use acceleration methods such as Aitken's extrapolation algorithm [69] to reduce the number of iterations necessary. This is shown for two combinations of values $(\widehat{b}/a, L/a)$ in Fig. 11, where it can be seen that less iterations are indeed required for convergence to the exact value, provided by Eq. (16). Note that L and a have to be of opposite sign for $b/a < 1$ in order for α_c to be positive. For values of $\widehat{b}/a > 1$ (Fig. 11, right), the fixed point iterative method diverges, while use of Aitken's algorithm still ensures convergence. Nevertheless, when used in the LES, values of β_c were observed to diverge even when using Aitken's method, i.e. the value of β_c (or equivalently α_c) was not converging to any value at least in some region of the LES numerical domain. Since the only difference, for a fixed timestep (implying frozen conditions of the values a, b and L) between Eqs. (23) and (17) is that
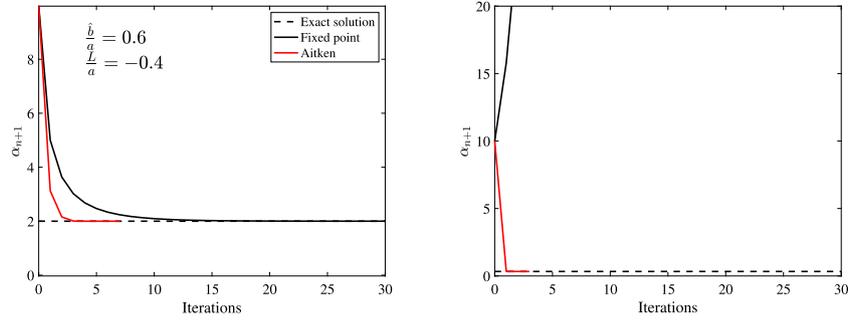
Fig. 11. Convergence of Eq. (22) to the exact solution $L/(\hat{b} - a)$ for different combinations of $\hat{b}/a$ and L/a. When $\hat{b}/a > 1$ (case on the right) the fixed point iteration diverges, while Aitken's method still provides convergence.
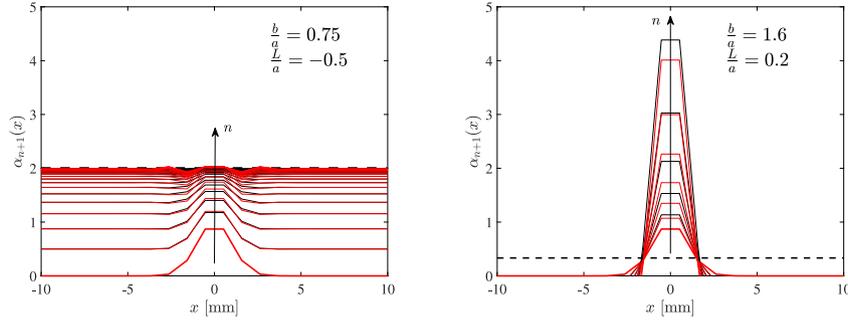

Fig. 12. Convergence of Eq. (24) towards the exact solution of Eq. (22) (--), given by $L/(\hat{b} - a)$ for two combinations of b/a and L/a. Solid lines indicates iterations with fixed point (——) and Aitken's acceleration method (——).

α_c is taken outside the filtering operation, the different behaviour in the LES must be due to the test-filtering operation, and/or the numerical noise associated by its application.

In order to estimate the error introduced by taking out the model constant from the test-filtering operator, one can expand $\hat{\alpha}_c$ and $\widehat{b\alpha_c}$ in series of Taylor using Eq. (20). Eq. (23), assuming $\hat{\Delta} = 2\Delta$, can then be rewritten as

$$\alpha_c \approx \frac{b}{a}\alpha_c - \frac{L}{a} + \frac{\Delta^2}{6}\left(\frac{1}{a}\frac{d^2(b\alpha_c)}{dx^2} - \frac{d^2(\alpha_c)}{dx^2}\right) \tag{23}$$

In order to have an estimation of the effect of the additional term on the right-hand side of Eq. (23), in first analysis it is assumed that a, b and L are constant (as before), and a Gaussian shape with amplitude 1 and width $\sigma = \delta_{th}$ is assigned across the flame to α_c as initial guess, where $\delta_{th} \approx 1$ mm is the laminar thermal flame thickness. Eq. (23) becomes:

$$\alpha_c \approx \frac{b}{a}\alpha_c - \frac{L}{a} + \frac{\Delta^2}{6}\frac{d^2\alpha_c}{dx^2}\left(\frac{b}{a} - 1\right) = \frac{b}{a}\alpha_c - \frac{L}{a} + \mathcal{T} \tag{24}$$

Two values for Δ where tested, $\Delta = \delta_{th}/10$ (representative of a resolved flame) and $\Delta = \delta_{th}$ (representative of the LES Case B). For both cases it is observed that, when the iterative method converges, it converges to the solution given by Eq. (22), which implies that the assumption herein of scale-invariance for α_c is not strong for LES filters up to the order of Δ. This is shown for the coarser filter width in Fig. 12. Nevertheless, convergence is relatively slow as compared to what was observed in Fig. 11, and the Aitken's method does not seem to accelerate convergence.

For $b/a > 1$ the iterative process, unlike what observed for Eq. (23), diverges even when using the Aitken's acceleration method, which is due to the sign change in the term $(b/a - 1)$ in Eq. (24). This demonstrates that the occurrence of instability in the computation of α_c (equivalently β_c) is to be found in the regions where $b/a > 1$ and $L/a > 0$ (the latter ensuring $\alpha_c > 0$). These regions have been extracted from the LES results with the differential test-filter and Eq. (16), for which the divergence issue does not manifest, and are highlighted for a random timestep in Fig. 13 for case B (bluffbody). As can be

noticed, there is a non-negligible region surrounding the flame where the iterative process would not converge ($b/a > 1$), which explains the observation made in the LES when β_c was computed iteratively. Another interesting aspect is that term $\mathcal{T}$ in Eq. (24) is lower in magnitude but of the same order of magnitude of the other two terms in the same equation. As the magnitude of $\mathcal{T}$ grows with the filter size Δ, one can expect that the same becomes the dominant term for filter sizes larger than δ_{th}, and different considerations might apply in that case. From the figure one can notice that the term b/a remains mostly positive in the region of the flame.

6. Conclusions

Large eddy simulations have been performed for a lifted jet flame in hot coflow and a bluff-body stabilized premixed flame using a flamelet/presumed PDF approach. The combustion modelling constant within the subgrid scalar dissipation rate (SDR) model, needed within the subgrid variance equation of progress variable, is estimated using a dynamic procedure and the assumption of scale similarity. A test-filtering operation based on a pseudo-Fourier differential equation has been proposed and associated results are compared to those obtained by using the standard algebraic approach based on explicit evaluation of a Gaussian filter shape. The two test-filters have been further tested on both block-structured and unstructured meshes in order to shed light on possible effects of non-orthogonality in the mesh, which results in numerical noise during the process of evaluation of the filter coefficients in the algebraic approach.

Results show that when a sufficient level of turbulence is present and the LES is well resolved, algebraic and differential filters predicts the same flow field if a block-structured mesh is used. This further indicates that the proposed differential filter method is able to mimic the correct results with great accuracy. When an unstructured mesh is used, by keeping the LES filter size about the same across the flame, the algebraic test-filter approach fails in estimating the correct flame position, which is observed to be due to an overestimation of the
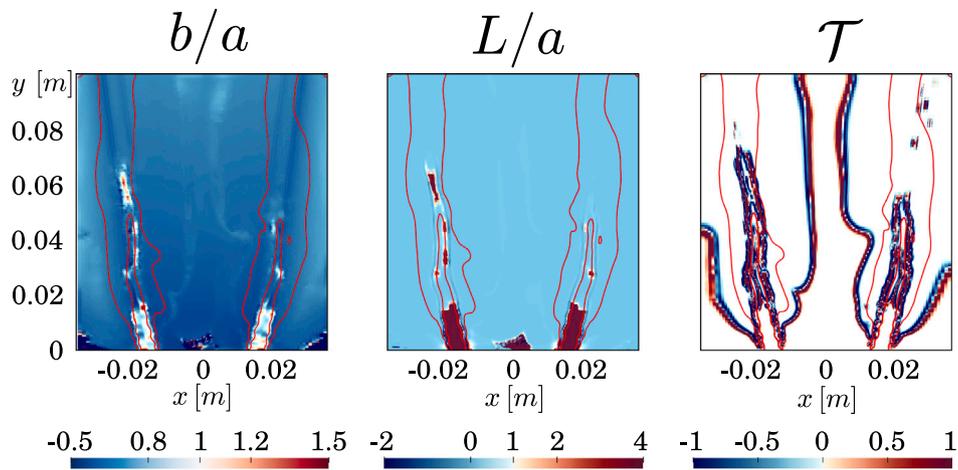
Fig. 13. Midplane contours at a random time of the various terms appearing in Eq. (24), as extracted from the LES of Case B with combustion constant $\beta_c = 1/\alpha_c$ computed using Eq. (16) and differential test-filter. Red isolines refer to $\widetilde{c} = 0.1$ and $\widetilde{c} = 0.9$, and are to mark the flame position.
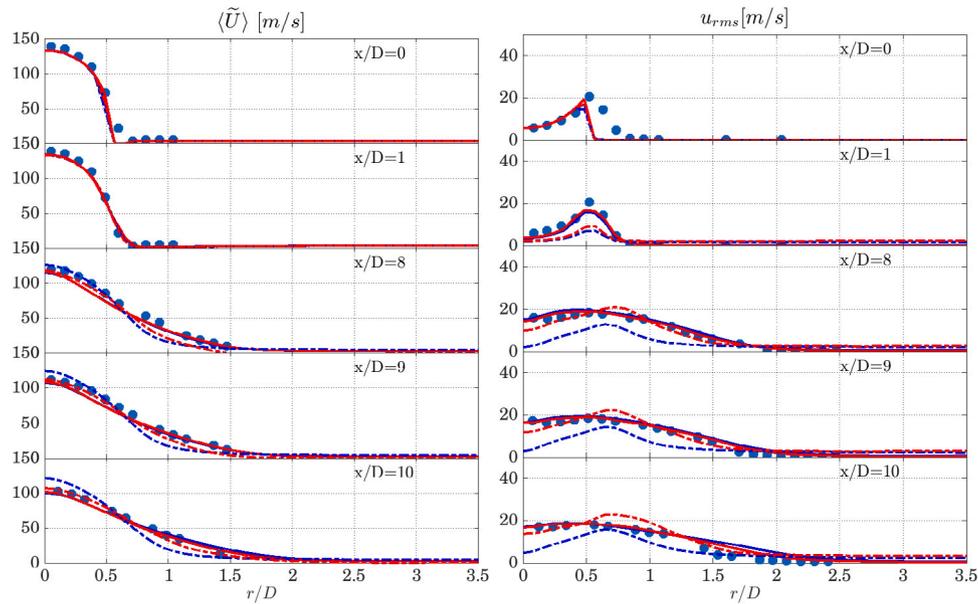

Fig. 14. Radial profiles of time averaged (left) and rms (right) axial velocity at different axial locations from experimental measurements (symbols) and LES: 1M cells BS mesh (—), 3M cells US mesh (- -), 8M cells BS mesh (—), and 8M cells US mesh (- -). All simulations refer to an integral length scale reported at the inlet of $l_0 = 0.07D$.
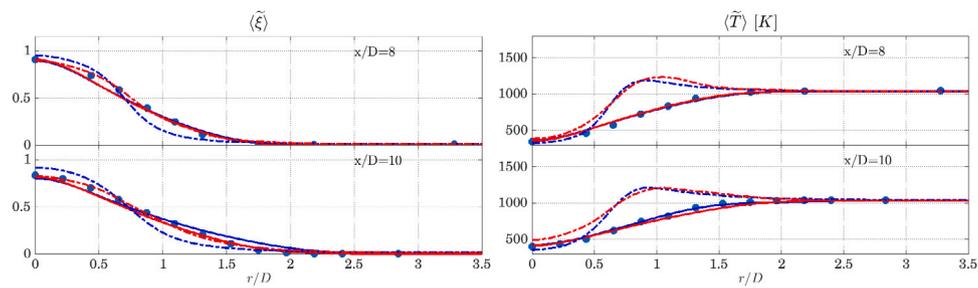

Fig. 15. Radial profiles of time averaged mixture fraction (left) and temperature (right) at different axial locations from experimental measurements (symbols) and LES. Legend is as for Fig. 14.
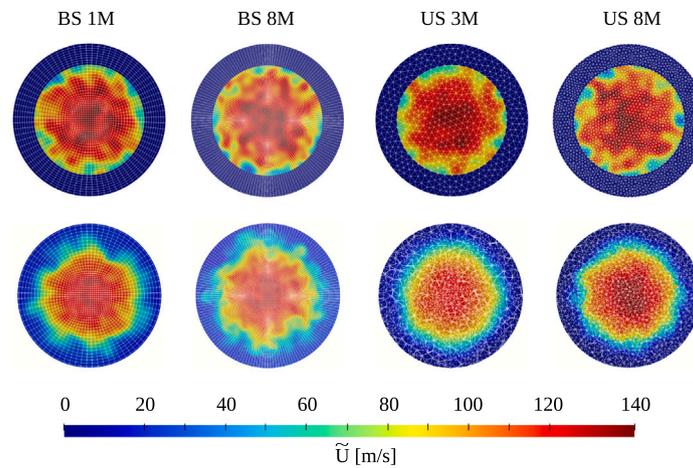
Fig. 16. Instantaneous velocity field at $x = 0D$ (top) and $x = 1D$ (bottom) for different meshes.

subgrid SDR, which in turns is due to underestimation of the modelling constant. On the contrary, the use of the differential filter allows to recover the correct flame position. It is believed that the algebraic test filter is affected by the noise produced by interpolation operations on the unstructured cells in the evaluation of the test-filter coefficients. This is not the case for the differential test-filter, where the solution is bounded to satisfy the differential equation.

In conditions of weak turbulence, it is observed that the algebraic test filter fails in the estimation of the correct values of the combustion modelling constant, resulting in an incorrect flame with laminar characteristics. On the other hand, the differential test-filter is still able to provide a meaningful range of values of the model constant, resulting in a wrinkled flame which better resembles that observed in experiments. These results indicate that the differential test-filter proposed here is more versatile that its algebraic counterpart, being able to deal with a much wider range of conditions and meshes, at the expense of an increased computational cost.

CRediT authorship contribution statement

Gioele Ferrante: Data curation, Formal analysis, Investigation, Methodology, Software, Validation, Visualization, Writing – original draft, Writing – review & editing. **Zhi X. Chen:** Conceptualization, Methodology, Software, Writing – original draft, Writing – review & editing . **Ivan Langella:** Conceptualization, Formal analysis, Investigation, Methodology, Project administration, Resources, Software, Supervision, Writing – original draft, Writing – review & editing.

Declaration of competing interest

The authors declare that they have no known competing financial interests or personal relationships that could have appeared to influence the work reported in this paper.

Data availability

Data will be made available on request.

Acknowledgements

Appendix. Mesh sensitivity for the lifted flame in hot coflow

Turbulence resolution is among the most sensitive aspects for the Cabra flame (test case A), as it affects the jet/coflow mixing and the intensity of the shear layer, ultimately determining the correct prediction of the jet flow features and flame stabilization. Moreover, the Cabra flame exhibits a strong sensitivity to the imposed turbulent boundary conditions. A mesh sensitivity is carried out in this section to provide some evidence on the above points. Note that by meaning of Pope's criterion (Fig. 2 in the main text) the 3M cells unstructured mesh has a degree of refinement which is comparable to the 1M cells block-structured grid in the region of the flame, as 80% of the turbulent kinetic energy is resolved in both cases.

In Figs. 14–15 the sensitivity of the computed statistics to the mesh refinement is reported for both the block-structured (BS) and unstructured (US) meshes. Note that, due to time limitation and limited resources, we have performed the additional simulations for the non-reactive case, implying comparisons with experiments are meaningful only upstream of the flame front (about $x = 11D$). The following observations are made:

- For the BS mesh, for which the 1M cells case yields already a good match with experiments, the predicted turbulent flow field appears to be almost insensitive to the mesh refinement.
- Refining the unstructured mesh from 3M to 8M cells does not lead to substantial differences in the turbulent velocity and temperature fields prediction, while some improvement is observed from the mixture fraction radial profiles. This suggests that numerical diffusion plays a stronger role on the US mesh as one would expect.
- The rms level at $1D$ obtained using the US meshes is underpredicted as compared to experiment, which leads to incorrect mixing further downstream. Given the strong sensitivity of the studied flame to the turbulence level upstream, the value of l_0 imposed at the inlet was changed in the simulations presented in Section 4 in order to ensure that the lift-off height would remain about the same as for the BS mesh in the reacting flow case.

Further indication of the effect of numerical diffusion is illustrated in Fig. 16, showing instantaneous contours of velocity field at two transversal locations, $x = 0D$ (nozzle exit), and $x = 1D$. Results show that at $x = 0D$, where the synthetic turbulence conditions are imposed,

similar turbulent characteristics are obtained on block-structured and unstructured meshes. Nevertheless, differences are clearly observable one diameter downstream, which is a result of stronger numerical diffusion in the unstructured mesh case and imposed integral length scale. This results suggest that to obtain the same level of turbulence resolution of the block-structured mesh one has to further refine the mesh in the unstructured case. This additional refinement is however not performed in this study since the objective is to compare algebraic and differential test-filters, which is performed at a fixed LES filter size. Nevertheless, the analysis above indicates that one has to be mindful when interpreting results obtained from block-structured and unstructured meshes.

References

[1] T.J. Poinsot, D. Veynante, Theoretical and Numerical Combustion, Edwards, 2005.

[2] O. Colin, F. Ducros, D. Veynante, T.J. Poinsot, A thickened flame model for large eddy simulations of turbulent premixed combustion, Phys. Fluids 12 (2000) 1843.

[3] S.H. Kim, H. Pitsch, Conditional filtering method for large-eddy simulation of turbulent nonpremixed combustion, Phys. Fluids 17 (10) (2005).

[4] R. Bilger, S. Pope, K. Bray, J. Driscoll, Paradigms in turbulent combustion research, Proc. Combust. Inst. 30 (1) (2005) 21–42.

[5] W.K. Bushe, H. Steiner, Conditional moment closure for large eddy simulation of nonpremixed turbulent reacting flows, Phys. Fluids 11 (7) (1999) 1896–1906.

[6] R. Bilger, Conditional moment closure for turbulent reacting flow, Phys. Fluids A: Fluid Dyn. 5 (2) (1993) 436–444.

[7] S. Pope, Computations of turbulent combustion: Progress and challenges, Proc. Combust. Inst. 23 (1990) 591–612.

[8] W. Jones, V. Prasad, Large eddy simulation of the sandia flame series (D–F) using the Eulerian stochastic field method, Combust. Flame 157 (9) (2010) 1621–1636.

[9] A. Avdić, G. Kuenne, F. Di Mare, J. Janicka, LES combustion modeling using the Eulerian stochastic field method coupled with tabulated chemistry, Combust. Flame 175 (2017) 201–219.

[10] K. Bray, M. Champion, P. Libby, N. Swaminathan, Finite rate chemistry and presumed PDF models for premixed turbulent combustion, Combust. Flame 146 (2006) 665–673.

[11] P. Domingo, L. Vervisch, D. Veynante, Large-eddy simulation of a lifted methane jet flame in a vitiated coflow, Combust. Flame 152 (2008) 415–432.

[12] A.N. Lipatnikov, V.A. Sabelnikov, An extended flamelet-based presumed probability density function for predicting mean concentrations of various species in premixed turbulent flames, Int. J. Hydrog. Energy 45 (55) (2020) 31162–31178.

[13] N. Peters, Laminar diffusion flamelet models in non-premixed turbulent combustion, Prog. Energy Combust. Sci. 10 (3) (1984) 319–339.

[14] J. Van Oijen, L. De Goey, Modelling of premixed laminar flames using flamelet-generated manifold, Combust. Sci. and Tech. 161 (2000) 113–137.

[15] J.A. Van Oijen, A. Donini, R.J.M. Bastiaans, J.H.M.T.T. Boonkkamp, L.P.H. De Goey, State-of-the-art in premixed combustion modeling using flamelet generated manifolds, Prog. Energy Combust. Sci. 57 (2016) 30–74.

[16] J. Duclos, D. Veynante, T. Poinsot, A comparison of flamelet models for premixed turbulent combustion, Combust. Flame 95 (1993) 101–117.

[17] L. Vervisch, D. Veynante, Interlinks between approaches for modeling turbulent flames, Proc. Combust. Inst. 28 (2000) 175–183.

[18] H. Pitsch, A consistent level set formulation for large-eddy simulation of premixed turbulent combustion, Combust. Flame 143 (4) (2005) 587–598.

[19] I. Langella, N. Swaminathan, Y. Gao, N. Chakraborty, Assessment of dynamic closure for premixed combustion LES, Combust. Theor. Model. 19 (2015) 628–656.

[20] I. Langella, Z.X. Chen, N. Swaminathan, S.K. Sadasivuni, Large-eddy simulation of reacting flows in industrial gas turbine combustor, J. Propul. Power 34 (2017) 1269–1284.

[21] I. Langella, N. Swaminathan, Unstrained and strained flamelets for LES of premixed combustion, Combust. Theor. Model. 20 (2016) 410–440.

[22] T. Dunstan, Y. Minamoto, N. Chakraborty, N. Swaminathan, Scalar dissipation rate modelling for large eddy simulation of turbulent premixed flames, Proc. Combust. Inst. 34 (2013) 1193–1201.

[23] F. Charlette, C. Meneveau, D. Veynante, A power-law flame wrinkling model for LES of premixed turbulent combustion, part I: Nondynamic formulation and initial tests, Combust. Flame 131 (2002) 159–180.

[24] R. Knikker, D. Veynante, C. Meneveau, *A priori* testing of a similarity model for large eddy simulations of turbulent premixed combustion, Proc. Combust. Inst. 29 (2002) 2105–2111.

[25] E. Knudsen, H. Pitsch, A dynamic model for the turbulent burning velocity for large eddy simulation of premixed combustion, Combust. Flame 154 (4) (2008) 740–760.

[26] H. Pitsch, Large-eddy simulation of turbulent combustion, Annu. Rev. Fluid Mech. 38 (2006) 453–482.

[27] Y. Gao, N. Chakraborty, N. Swaminathan, Algebraic closure of scalar dissipation rate for large eddy simulations of turbulent premixed combustion, Combust. Sci. Technol. (2014).

[28] P. Volpiani, T. Schmitt, D. Veynante, A posteriori tests of a dynamic thickened flame model for large eddy simulations of turbulent premixed combustion, Combust. Flame 174 (2016) 166–178.

[29] V. Moureau, B. Fiorina, H. Pitsch, A level set formulation for premixed combustion LES considering the turbulent flame structure, Combust. Flame 156 (4) (2008) 801–812.

[30] G.I. Park, M. Bassenne, J. Urzay, P. Moin, A simple dynamic subgrid-scale model for LES of particle-laden turbulence, Phys. Rev. Fluids 2 (2017) 044301.

[31] X. Chai, K. Mahesh, Dynamic k-equation model for large eddy simulation of compressible flow, J. Fluid Mech. 699 (2012) 385–413.

[32] I. Langella, N. Swaminathan, Y. Gao, N. Chakraborty, LES of premixed combustion: Sensitivity to SGS velocity modelling, Combust. Sci. Technol. 189 (2015) 43–78.

[33] J.F. Driscoll, J.H. Chen, A.W. Skiba, C.D. Carter, E.R. Hawkes, H. Wang, Premixed flames subjected to extreme turbulence: Some questions and recent answers, Prog. Energy Combust. Sci. 49 (2020) 189–208.

[34] A.N. Hernández-Pérez, V.A. Sabelnikov, F.E. Hernández-Pérez, W. Song, H.G. Im, *A priori* DNS study of applicability of flamelet concept to predicting mean concentrations of species in turbulent premixed flames at various karlovitz numbers, Combust. Flame 222 (2020) 370–382.

[35] R.W. Bilger, S.H. Stårner, R.J. Kee, On reduced mechanism for methane-air combustion in nonpremixed flames, Combust. Flame 80 (1990) 135–149.

[36] J.D. Regele, E. Knudsen, H. Pitsch, G. Blanquart, A two-equation model for non-unity Lewis number differential diffusion in lean premixed laminar flames, Combust. Flame 160 (2) (2013) 240–250.

[37] N. Mukundakumar, D. Efimov, N. Beishuizen, J. Van Oijen, A new preferential diffusion model applied to FGM simulations of hydrogen flames, Combust. Theory Model. 25 (7) (2021) 1245–1267.

[38] I. Langella, N. Swaminathan, R.W. Pitz, Application of unstrained flamelet SGS closure for multi-regime premixed combustion, Combust. Flame 173 (2016) 161–178.

[39] B. Fiorina, R. Baron, O. Gicquel, D. Thevenin, S. Carpentier, N. Darabiha, Modelling non-adiabatic partially premixed flames using flame-prolongation of ILDM, Combust. Theor. Model. 7 (2003) 449–470.

[40] D. Veynante, L. Vervisch, Turbulent combustion modeling, Prog. Energy Combust. Sci. 28 (3) (2002) 193–266.

[41] Z.X. Chen, N.A.K.D. Doan, S. Ruan, I. Langella, N. Swaminathan, A priori investigation of subgrid correlation of mixture fraction and progress variable in partially premixed flames, Combust. Theor. Model. 22 (5) (2018) 862–882.

[42] Z.X. Chen, I. Langella, R.S. Barlow, N. Swaminathan, Prediction of local extinctions in piloted jet flames with inhomogeneous inlets using unstrained flamelets, Combust. Flame 212 (2020) 415–432.

[43] M. Ihme, C.M. Cha, H. Pitsch, Prediction of local extinction and re-ignition effects in non-premixed turbulent combustion using a flamelet/progress variable approach, Proc. Combust. Inst. 30 (1) (2005) 793–800.

[44] A. Soli, I. Langella, Z.X. Chen, Analysis of flame front breaks appearing in LES of inhomogeneous jet flames using flamelets, Prog. Energy Combust. Sci. 49 (2021) 189–208.

[45] S.B. Pope, Turbulent Flows, Cambridge University Press, 2000.

[46] M. Germano, U. Piomelli, P. Moin, W.H. Cabot, A dynamic subgrid-scale eddy viscosity model, Phys. Fluids A 3 (7) (1991) 1760.

[47] F. Charlette, C. Meneveau, D. Veynante, A power-law flame wrinkling model for LES of premixed turbulent combustion, part II: dynamic formulation, Combust. Flame 131 (2002) 181–197.

[48] S.R. Gubba, S.S. Ibrahim, W. Malalasekera, Dynamic flame surface density modelling of flame deflagration in vented explosion, Combust. Explos. Shock Waves 48 (2012) 393–405.

[49] R. Knikker, D. Veynante, C. Meneveau, A dynamic flame surface density model for large eddy simulations of turbulent premixed combustion, Phys. Fluids 16 (2004) 91.

[50] G. Wang, M. Boileau, D. Veynante, K. Truffin, Large eddy simulation of a growing turbulent premixed flame kernel using a dynamic flame surface density model, Combust. Flame 159 (8) (2012) 2742–2754.

[51] V. Moureau, P. Domingo, L. Vervisch, From large-eddy simulation to direct numerical simulation of a lean premixed swirl flame: Filtered laminar flame-pdf modeling, Combust. Flame 158 (5) (2011) 1340–1357.

[52] R. Cabra, T. Myhrvold, J.Y. Chen, R.W. Dibble, A.N. Karpetis, R.S. Barlow, Simultaneous laser Raman-Rayleigh-LIF measurements and numerical modeling results of a lifted turbulent H_2/N_2 jet flame in a vitiated coflow, Proc. Combust. Inst. 29 (2002) 1881–1888.

[53] J.R. Dawson, R.L. Gordon, J. Kariuki, E. Mastorakos, A.R. Masri, M. Juddoo, Visualization of blow-off events in bluff-body stabilized turbulent premixed flames, Proc. Combust. Inst. 33 (2011) 1559–1566.

[54] N.W. Bressloff, A parallel pressure implicit splitting of operators algorithm applied to flows at all speeds, Internat. J. Numer. Methods Fluids 36 (2001) 497–518.

[55] J. Ferziger, M. Peric, Computational Methods for Fluid Dynamics, Springer, 1999.

[56] S.B. Pope, Ten questions concerning the large-eddy simulation of turbulent flows, New J. Phys. 6 (2004).

[57] N. Kornev, E. Hassel, Method of random spots for generation of synthetic inhomogeneous turbulent fields with prescribed autocorrelation functions, Commun. Numer. Methods Eng. 23 (1) (2007) 35–43.

[58] R.R. Cao, S.B. Pope, A.R. Masri, Turbulent lifted flames in a vitiated coflow investigated using joint PDF calculations, Combust. Flame 142 (4) (2005) 438–453.

[59] R. Gordon, S. Starner, A. Masri, R. Bilger, Further characterisation of lifted hydrogen and methane flames issuing into a vitiated coflow, in: Proceedings of the 5th Asia-Pacific Conference on Combustion, 2005, pp. 333–336.

[60] Z. Wu, A.R. Masri, R.W. Bilger, An experimental investigation of the turbulence structure of a lifted H_2/N_2 jet flame in a vitiated co-flow, Flow. Turbul. Combust. 76 (1) (2006) 61–81.

[61] D.B. Spalding, A single formula for the law of the wall, J. Appl. Mech. 28 (3) (1961) 455–458.

[62] CHEM1D, A One-Dimensional Laminar Flame Code, Eindhoven University of Technology.

[63] (GRI), T.: GRI-Mech 3.0. URL http://www.me.berkeley.edu/gri_mech/.

[64] Chemical-Kinetic Mechanisms for Combustion Applications, San Diego Mechanism web page, Mechanical and Aerospace Engineering (Combustion Research), University of California at San Diego, 2023, URL http://combustion.ucsd.edu. Last Accessed 06 October 2023.

[65] R. Cabra, J.Y. Chen, R.W. Dibble, A.N. Karpetis, R.S. Barlow, Lifted methane-air jet flames in a vitiated coflow, Combust. Flame 143 (4) (2005) 491–506.

[66] L. Selle, G. Lartigue, T. Poinsot, R. Koch, K.-U. Schildmacher, W. Krebs, B. Prade, P. Kaufmann, D. Veynante, Compressible large eddy simulation of turbulent combustion in complex geometry on unstructured meshes, Combust. Flame 137 (4) (2004) 489–505.

[67] I. Langella, N. Swaminathan, F.A. Williams, J. Furukawa, Large-eddy simulation of premixed combustion in the corrugated-flamelet regime, Combust. Sci. Technol. 188 (9) (2016) 1565–1591.

[68] J.C. Massey, I. Langella, N. Swaminathan, Large eddy simulation of a bluff body stabilised premixed flame using flamelets, Flow Turbul. Combust. 101 (2018) 973–992.

[69] K. Atkinson, An Introduction to Numerical Analysis, John wiley & sons, 1991.